AIP | Physics of Plasmas

Impact of screening of resonant magnetic perturbations in three dimensional edge plasma transport simulations for DIII-D

H. Frerichs, D. Reiter, O. Schmitz, P. Cahyna, T. E. Evans et al.

Citation: Phys. Plasmas **19**, 052507 (2012); doi: 10.1063/1.4714616
View online: http://dx.doi.org/10.1063/1.4714616
View Table of Contents: http://pop.aip.org/resource/1/PHPAEN/v19/i5
Published by the American Institute of Physics.

Impact of screening of resonant magnetic perturbations in three dimensional edge plasma transport simulations for DIII-D

H. Frerichs,[1] D. Reiter,[1] O. Schmitz,[1] P. Cahyna,[2] T. E. Evans,[3] Y. Feng,[4] and E. Nardon[5]
[1]*Institute of Energy and Climate Research—Plasma Physics, Forschungszentrum Jülich GmbH, Association EURATOM-FZJ, Partner in the Trilateral Euregio Cluster, Jülich, Germany*
[2]*Institute of Plasma Physics AS CR, v.v.i., Association EURATOM/IPP.CR, Prague, Czech Republic*
[3]*General Atomics, P.O. Box 85608, San Diego, California 92186-5608, USA*
[4]*Max-Planck Institute for Plasma Physics, Greifswald, Germany*
[5]*Association EURATOM-CEA, IRFM, CEA Cadarache, St-Paul-lez-Durance, France*

(Received 7 November 2011; accepted 11 April 2012; published online 22 May 2012)

The impact of resonant magnetic perturbations (RMPs) on the plasma edge can be analyzed in detail by three dimensional computer simulations, which take the underlying magnetic field structure as input. Previously, the "vacuum approximation" has been used to calculate the magnetic field structure although plasma response effects may result in a screening (or even an amplification) of the external perturbations. Simulation results for an ITER similar shape plasma at the DIII-D tokamak are presented for the full vacuum perturbation field and an ad hoc screening case in comparison to the unperturbed configuration. It is shown that the RMP induced helical patterns in the plasma edge and on the divertor target shrink once screening is taken into account. However, a flat temperature profile is still found in the "open field line domain" inside the separatrix, while the "density pump out effect" found in the vacuum RMP case is considerably weakened.
[http://dx.doi.org/10.1063/1.4714616]

I. INTRODUCTION

Resonant magnetic perturbations (RMPs) are applied at the plasma edge of several magnetically confined fusion experiments and are under consideration for ITER as well. Resulting 3D effects on the edge plasma have been reported, e.g., at DIII-D,[1,2] TEXTOR,[3,4] NSTX,[5] JET, and MAST.[6] The recent interest in RMPs is caused by their beneficial impact on intrinsic edge instabilities (ELMs) in high confinement (H-mode) plasmas: the application of RMPs can mitigate or even suppress ELMs, as demonstrated at DIII-D (Refs. 7 and 8) and JET (Ref. 9), and recently also at ASDEX Upgrade.[10] Such an option could be of vital interest for the ITER divertor, because extrapolations show that the ELM induced large transient heat fluxes will significantly reduce the wall life time.[11]

However, the detailed physical mechanisms in RMP edge plasmas are still not entirely understood quantitatively. Recent simulations for RMP H-mode plasmas at DIII-D have shown a significant striation pattern in both particle and heat fluxes to the divertor target,[12] but such a strong heat flux striation is not observed in the corresponding experiment.[2] Furthermore, a strong temperature reduction at the plasma edge by RMPs is found in simulations[13] but not in the experiment. While the edge plasma is considerably modified by RMPs, the plasma itself can modify the magnetic perturbation field as well (plasma response), which might be a solution for this mismatch. The plasma response is often neglected (in the so called vacuum approximation) in 3D simulations of the plasma edge (such as for DIII-D,[12,13] NSTX (Ref. 14), and ASDEX Upgrade[15]) but is now taken into account by the ansatz presented in Ref. 16 of introducing ad hoc helical current sheets on resonant magnetic surfaces. As there are indications that RMPs are (partially) screened inside the plasma,[17–19] we consider the case of weak RMP penetration and compare this to the extreme cases of full penetration (i.e., no screening, the vacuum approximation) and full screening (i.e., the axisymmetric configuration without RMPs).

We begin with an analysis of the magnetic field configuration in Sec. II for an ITER similar shape plasma (regarding elongation and triangularity) at the DIII-D tokamak. Both the unmodified vacuum magnetic perturbation and the screened perturbation are used to calculate the corresponding magnetic field configuration, which is then used in Sec. III as input for 3D edge plasma transport simulations with the EMC3-EIRENE code.[20,21] This code applies a fluid transport model for the edge plasma, which is coupled to a kinetic transport model for neutral particles. Originally developed for stellarators, it has also been used to study 3D effects by RMPs at the TEXTOR tokamak[4,22–24] and then generalized for the application in poloidally diverted tokamak configurations.[25] After a short description of the input parameters for this code, the resulting impact of RMP screening on the edge plasma, in particular on particle and heat fluxes to the divertor targets, is discussed. While screening of RMPs has already been considered in effective 1D transport models,[26] the present approach allows for a realistic 3D treatment and to resolve the spatial distribution of divertor particle and heat fluxes.

II. MAGNETIC FIELD CONFIGURATION

The following analysis of the magnetic field configuration and edge plasma transport is based on an ITER similar shape plasma at the DIII-D tokamak (elongation $\kappa \approx 1.8$ and average triangularity $\delta \approx 0.5$): discharge 132 741 at 3760 ms. This discharge is characterized by a plasma current

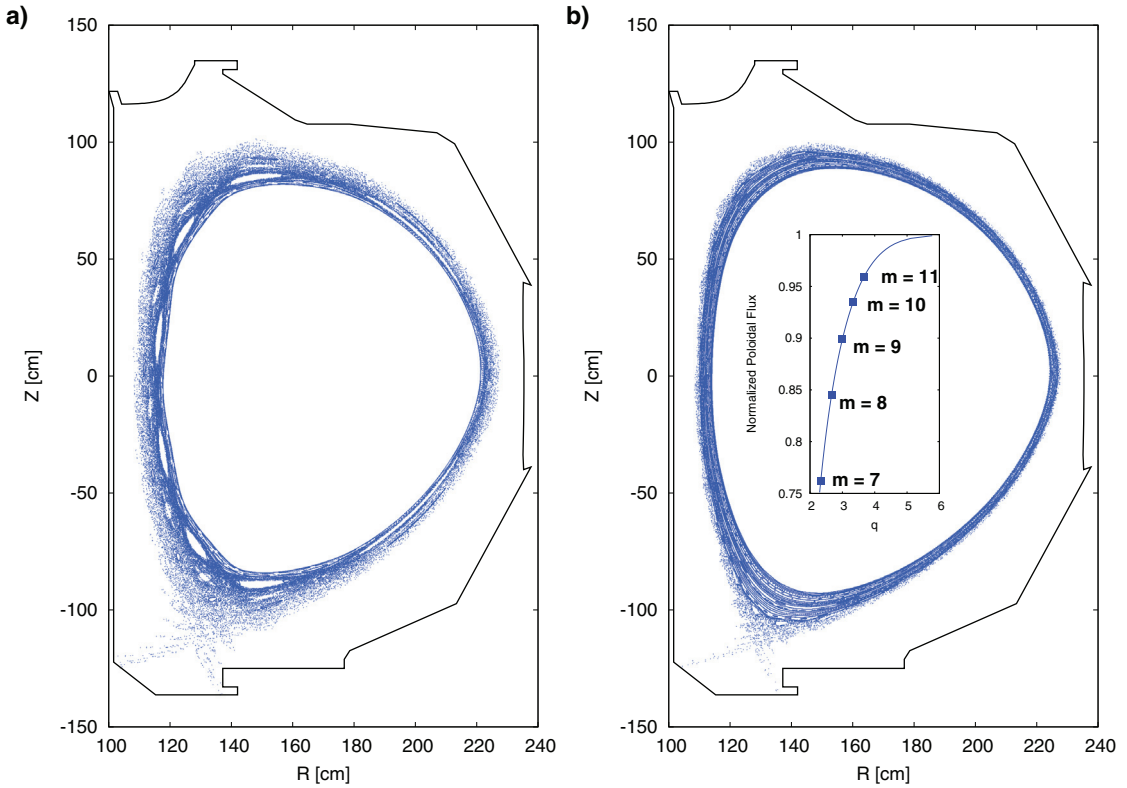

FIG. 1. Poincaré plot of (a) the vacuum field configuration and (b) plasma response configuration. The radial profile of the safety factor q is shown in the inset of (b).

of $I_p = 1.5$MA and a toroidal magnetic field of $B_t = 1.8$T at the vessel centre. The safety factor at 95% of the normalized poloidal flux is $q_{95} \equiv q(\Psi_N = 0.95) = 3.52$. The resonant magnetic perturbation field is provided by the I-coils (a set of six upper and lower rectangular coils located at the low field side of the machine), which are powered by $I_c = 4$kA in an even configuration (same current direction in each pair of upper and lower coil) with toroidal base mode number $n = 3$. Error fields and their corrections are neglected at this point. A Poincaré plot for the vacuum RMP configuration is shown in Figure 1(a).

In order to mimic a plasma response, we apply helical current sheets (which are phase aligned with the external field) at the plasma edge on resonant surfaces with poloidal mode number $m = 7$–11. The current sheets are tuned for a maximal screening of the corresponding modes of the externally applied perturbation field on these surfaces (which are located between $\Psi_N = 0.76$ and $\Psi_N = 0.96$). Details of this method are presented in Ref. 16 with examples for COMPASS and JET including an estimate of the numerical error. In the present case, we use 4096 filaments for a discretization of each current sheet. In the future, we plan to link the choice of screening surfaces (and screening factors allowing for incomplete screening) to MHD modeling of the plasma response to RMPs.

A Poincaré plot of the resulting field configuration is shown in Figure 1(b). The same plot is shown in blue in Figure 2(a) with a focus on the edge region in comparison to the vacuum field configuration in red. It can be seen that the last closed magnetic flux surface in the case with plasma response is pushed outward to $\Psi_N \approx 0.96$, which is determined by the outermost screening surface, while for the case with vacuum perturbation field, it is located at $\Psi_N \approx 0.79$. Outside of $\Psi_N \approx 0.96$, a domain with "open field lines" connecting to solid surfaces stays, even in our case with "strong plasma response." In particular, a perturbation of the separatrix

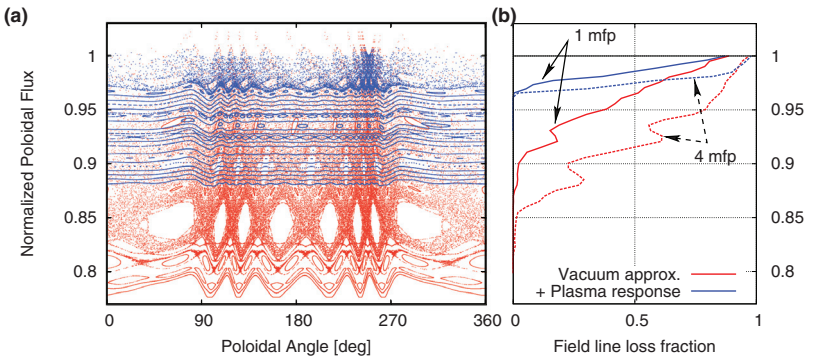

FIG. 2. (a) Poincaré plot of the vacuum field configuration (red) and plasma response configuration (blue) at $\varphi = 0$ deg. (b) Radial dependence of field line losses within one λ_{mfp} (solid lines) and 4 λ_{mfp} (dashed lines).

persists as well, which will be discussed below. Furthermore, it can be seen that screening within $\Psi_N = 0.96$ is not perfect, but small island chains persist, e.g., the $m = 10$ island chain at $\Psi_N = 0.94$ and some higher order island chains. This imperfect screening is related to the finite discretization of the helical current sheets and the singular behavior of the island width d at small remaining perturbations δB (i.e., $d \sim \sqrt{\delta B}$).

For the subsequent analysis of plasma transport in these magnetic field configurations, we introduce a measure for the "openness" of the plasma edge: the field line loss fraction Ξ.[27] $\Xi(\Psi_N)$ is calculated by distributing initial points in toroidal and poloidal direction on an unperturbed flux surface at Ψ_N. Then, we carry out field line tracing from these initial points and calculate the fraction of field lines lost to the wall. Field line tracing is stopped after some finite cut-off length $L_{\max}$. We choose two different values for $L_{\max}$ guided by the mean free path for electrons λ_{mfp}: $L_{\max,1} = \lambda_{\mathrm{mfp}}$ and $L_{\max,2} = 4\lambda_{\mathrm{mfp}}$, where λ_{mfp} is evaluated for $n_e = 10^{19}\mathrm{m}^{-3}$ and $T_e = 650$ eV (the reason for this choice will become clear later). It can be seen in Figure 2(b) that significant field line losses occur on a few λ_{mfp} in the plasma response case just outside the last closed flux surface.

Another impact of the "plasma response" is a modification of the helical lobe structure, which is formed by the separatrix manifolds.[1,2,12] This is shown in Figure 3 by the local field line connection length L_c at a cross-section in the X-point region and at the inner strike point. The helical lobes are much shorter in the case with plasma response, which indicates that a less pronounced pattern will be imprinted on the edge plasma as well. The size of the magnetic footprint depends on the number of screening surfaces (as shown for COMPASS and JET using the Melnikov function[16]) and will further diminish if more screening surfaces are included, e.g., at $m = 12, 13, \ldots$, or increase if fewer screening surfaces are selected. Two other examples of a "plasma response" are shown in Figure 4: (a) screening on the $m = 9$–11 surfaces and (b) screening on a single surface at $m = 9$. The direct comparison of the footprint of the $m = 9$–11 screening case with the $m = 7$–11 one in Figure 3(b) shows that the size of the footprint is only weakly affected by the inner resonances

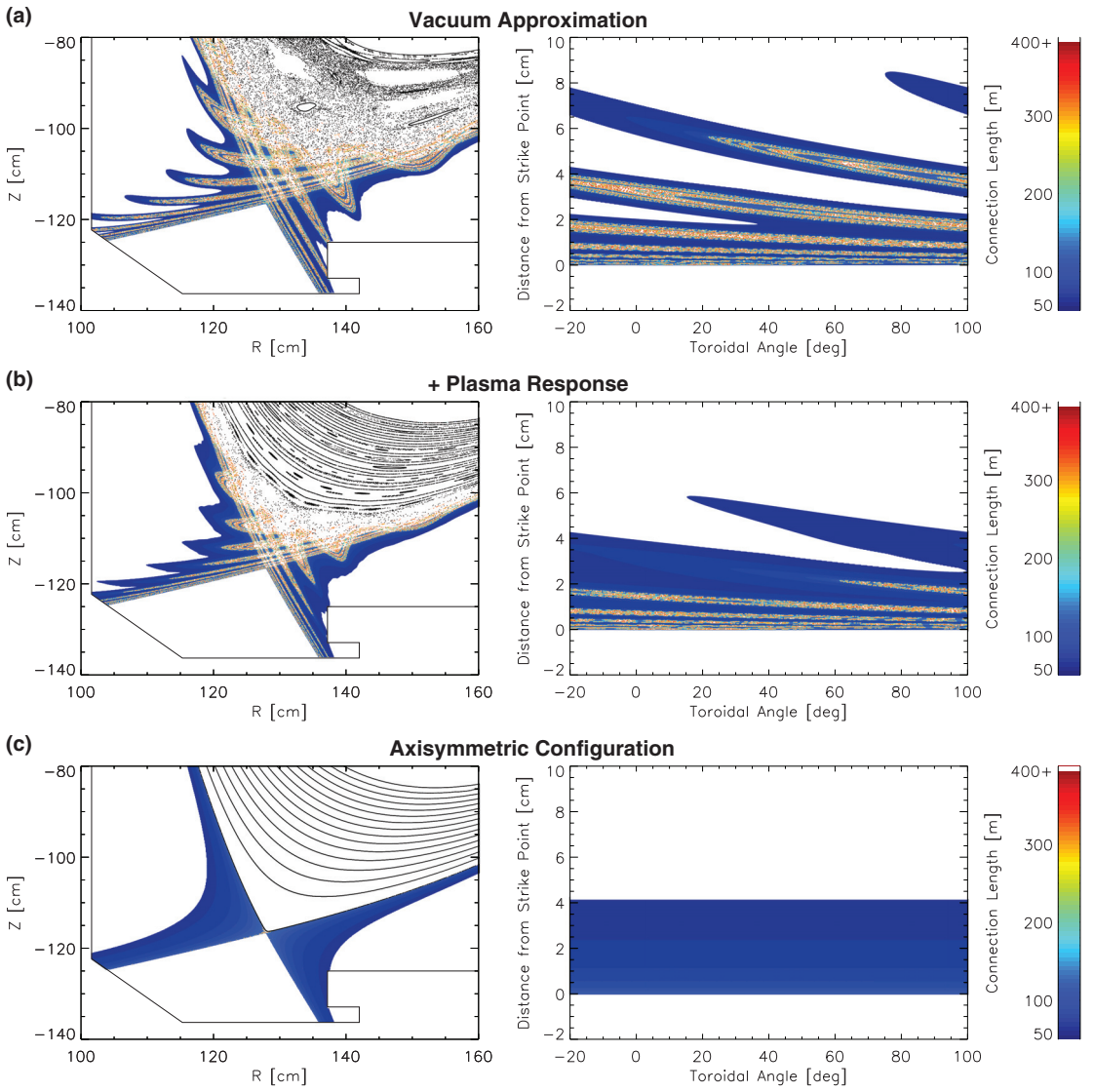

FIG. 3. Field line wall to wall connection length L_c at a poloidal cut at $\varphi = 0$ deg in the X-point region (left column) and at the inner strike point (right column) for (a) the vacuum approximation, (b) the plasma response case, and (c) the axisymmetric configuration without perturbations.

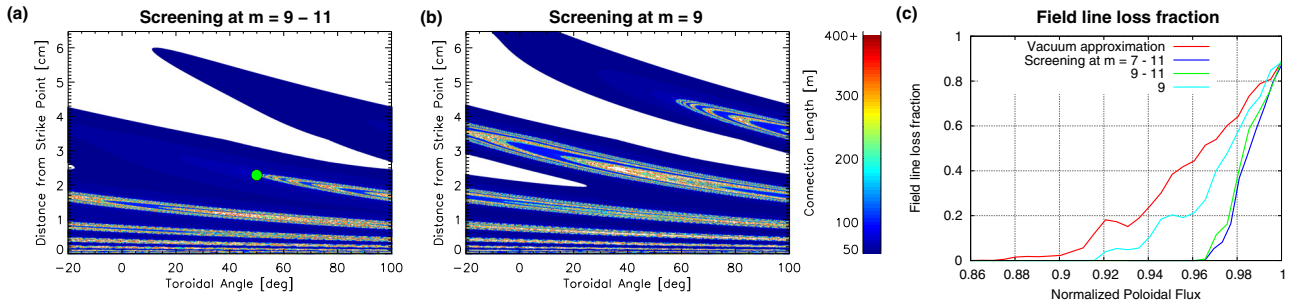

FIG. 4. Connection length at the inner strike point: (a) with screening at the $m = 9$–11 surfaces and (b) at a single surface at $m = 9$. (c) Field line loss fractions within $L_{\max} = \lambda_{\mathrm{mfp}}$.

at $m = 7$ and 8: The tip of the perturbed separatrix (marked by the green dot) is shifted from $\Delta L_{m=9-11} = 2.3$ cm at $\varphi = 50$ deg to $\Delta L_{m=7-11} = 2.2$ cm at $\varphi = 60$ deg. The beginning of field line loss region is determined by the outermost screening surface which is in both cases located at $m = 11$, but the magnitude of field line losses is slightly increased if the inner resonances are present (see Figure 4(c)). On the other hand, a single screening surface can already make a big difference, for the size of the footprint as well as the beginning of the open field line region: The tip of the perturbed separatrix at $\Delta L_{\mathrm{vac}} = 5.7$ cm and $\varphi = 20$ deg in the vacuum approximation is pulled back to $\Delta L_{m=9} = 4.5$ cm at $\varphi = 60$ deg (see Figure 4(b) and the last closed magnetic flux surfaces is pushed outward to $\Psi_N = 0.91 - 0.92$.

The main part of the unperturbed (no RMPs) scrape-off layer (SOL) is characterized by a connection length of $L_c \gtrsim 50$ m (blue), while $L_c \lesssim 50$ m in the far SOL only (white). The radial width of the main SOL is $\Delta R = 7$ mm at the HFS midplane, which expands to $\Delta L = 4$ cm (along the wall) at the inner strike point. In the presence of RMPs, this thin layer (i.e., the blue domain in Figure 3) is wrapped around the separatrix manifolds, which leads to an expansion of the helical magnetic footprint (up to $\Delta L = 8.5$ cm at $\varphi = 75$ deg for the vacuum approximation and $\Delta L = 6$ cm at $\varphi = 15$ deg for the "plasma response" case). It can be expected that significant particle and heat fluxes onto surface structures will develop in these regions as well, fed by cross-field transport into this thin layer. This suggests, in combination with the magnetic footprint pattern for the ITER divertor calculated in Ref. 28, that particle and heat fluxes might also reach the tungsten tiles region, despite a restriction of the main helical lobes to the graphite tiles region.

III. EDGE PLASMA SIMULATIONS

The edge plasma transport model in the EMC3-EIRENE code is based on a set of steady state fluid equations. Transport parallel to magnetic field lines is considered within the classical transport theory by Braginskii,[29] while anomalous cross-field transport is taken into account by free model parameters for particle ($D_\perp$) and electron and ion heat transport (χ_e and χ_i, respectively). These parameters are set to $D_\perp = 0.2$ m^2 s^{-1} and $\chi_e = \chi_i = 0.6$ m^2 s^{-1} throughout this present work. Earlier simulations have shown that such low values are required in order to obtain pronounced striation patterns on the divertor target[12] (which are indeed observed experimentally, at least for the particle flux). The code requires a field aligned grid for a fast reconstruction of magnetic field lines (see Ref. 25 for details) and the corresponding grid generator has been advanced to include the magnetic field generated by current sheets.

A closed, perturbed magnetic surface at $\Psi_N = 0.78$ is taken as inner simulation boundary (ISB). The total particle Γ_{ISB} and energy input P_{ISB} across this surface are set as boundary conditions for the code. The values of $\Gamma_{\mathrm{ISB}} = 1.1 \cdot 10^{21}$ s^{-1} and $P_{\mathrm{ISB}} = 6.3$ MW have been taken from earlier simulations[13] based on similar experimental conditions.

The resulting spatial profiles of electron density n_e and temperature T_e in the X-point region are shown in Figure 5. As already suggested by the magnetic field structure analysis above, the helical lobe pattern of the edge plasma n_e and T_e is much weaker (i.e., shorter excursion of the lobes) in the "plasma response" case than in the vacuum approximation. The clear alignment of the n_e and T_e pattern with the underlying magnetic field structure is caused by the fast parallel transport compared to cross-field transport. Because of the very high parallel electron heat conductivity, the impact of open field lines on T_e is much stronger than on n_e: a large temperature reduction with respect to the unperturbed case is found throughout the plasma edge.

A. Midplane profiles

Radial profiles are extracted at the LFS midplane in Figure 6 for a more detailed analysis. Because of the uncertainty regarding the anomalous cross-field transport in the simulations—in particular, the missing edge transport barrier effects in the present model—we do not show experimental profiles in comparison to the numerical ones, but rather discuss the respective tendencies. It can be seen that the T_e profile in the vacuum approximation (green line) is flat in the entire region with open field lines, at a level of $T_e \approx 600 - 650$ eV. This is a significant reduction compared to the axisymmetric case (red line), but this is not observed in the corresponding experiment (only -30% at $\Psi_N = 0.8$, see Figure 1 in Ref. 30). The temperature reduction at $\Psi_N = 0.8$ in the "plasma response" case (blue line), on the other hand, is only -12%, but a significant temperature reduction is also found in the open field line region (there, however, this open field line region is restricted further to the edge). The slope of the T_e profile is steep in the confined region with a sharp transition at the last closed flux surface. The

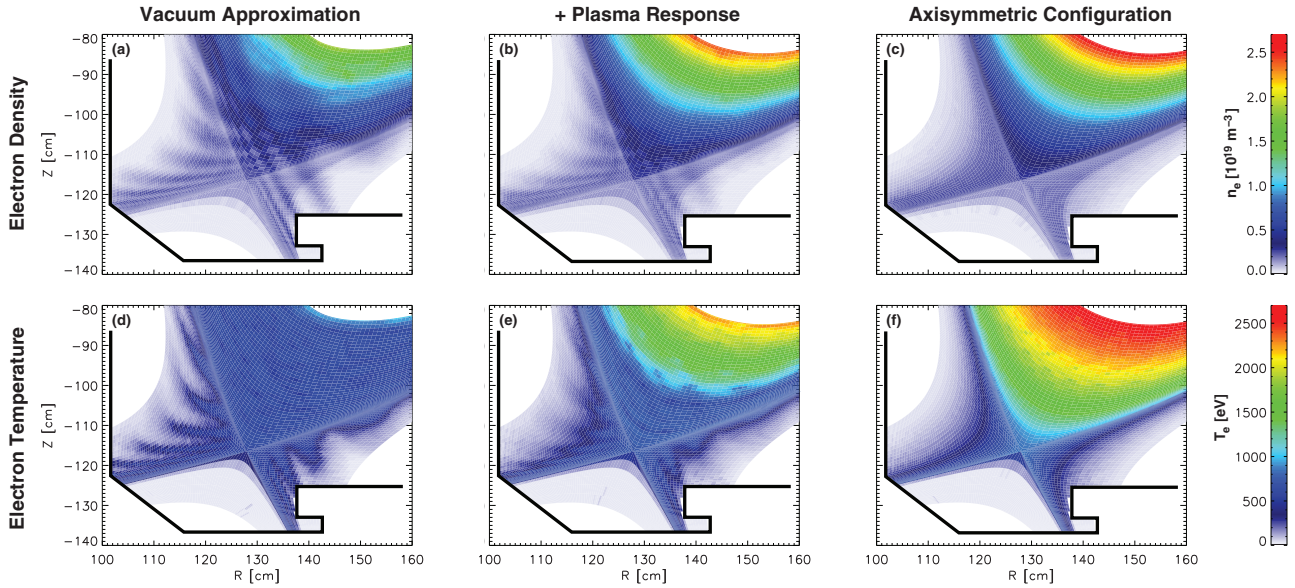

FIG. 5. 2D cuts of plasma parameters at $\varphi = 0$ deg: (a)–(c) electron density and (d)–(f) electron temperature for the vacuum approximation, the plasma response case, and the axisymmetric configuration.

reason for this sharp transition is that as one moves radially outward across this particular position, immediately a significant fraction of field lines intersect the divertor target within a few electron mean free paths (see Figure 2(b)). In the vacuum approximation, however, the field lines loss fraction increases much more smoothly with radial position.

While parallel heat convection is supplemented by the very powerful parallel heat conduction, there is no other parallel particle transport mechanism than directional flow. Therefore, the impact of RMPs on the density is much weaker, both in the vacuum approximation and in the "plasma response" case. In the latter case, the density is almost restored up to the level of the axisymmetric configuration. In particular the experimentally observed density pump out (density reduction of factor 2 at $\Psi_N = 0.8$, see Figure 1 in Ref. 30) is not found in the simulation. This observation, and the flat T_e profiles, suggest that (at least for the current assumption of prescribed cross-field diffusion coefficients in the code) the present RMP screening ansatz overestimates the plasma response effect, while kinetic corrections to the parallel electron heat conductivity in the fluid model are most probably required. However, we keep in mind that there are indications that the radial electric field is modified during RMP application,[31,32] resulting in a modification of cross-field transport as well.

B. Divertor particle and heat loads

The distribution of divertor particle and heat loads (Γ_{target} and q_{target}, respectively) is modified as well, if a plasma response is taken into account. As can be seen in Figure 7 for the inner strike point (ISP), the pattern of the target loads is in both cases aligned to the corresponding magnetic field structure in Figure 3. In general, the heat flux decays much faster than the particle flux, which is related to the different source type: power sources are located in the core (i.e., at the inner simulation boundary), while there is a large contribution to particle sources by the recycling flux in the SOL. Both particle and heat fluxes in the "plasma response" case are more concentrated at the main strike point at $\Delta L = 0$, and the main peak increases by $\Delta\Gamma_{\text{target}} = 17\%$ and $\Delta q_{\text{target}} = 35\%$ with respect to the vacuum approximation. However, a significant splitting of the target loads persists in the "plasma response" case. In particular, a pronounced secondary peak in the target heat flux is found in the simulations but not so much in corresponding experiments.[28] Nevertheless, the reduction of the secondary heat flux peak (at $\Delta L \approx 3$ cm) in the "plasma response" case is stronger (-30%) than the reduction of the secondary particle flux peak (-17%), which is at least the correct tendency regarding experimental observations.

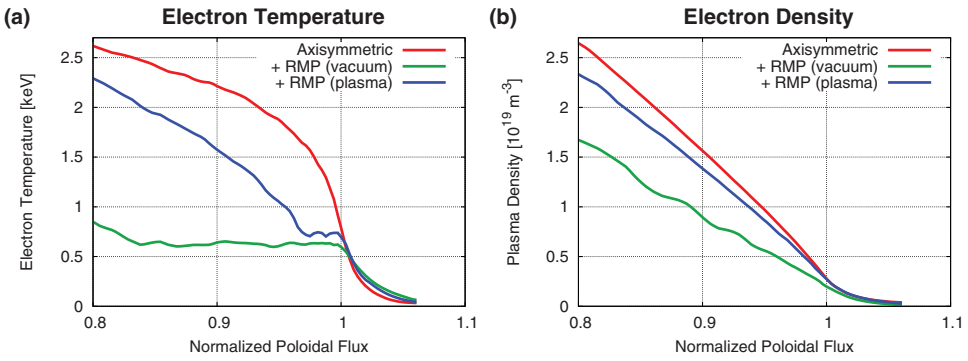

FIG. 6. Radial profiles at the LFS midplane: (a) electron temperature and (b) electron density.

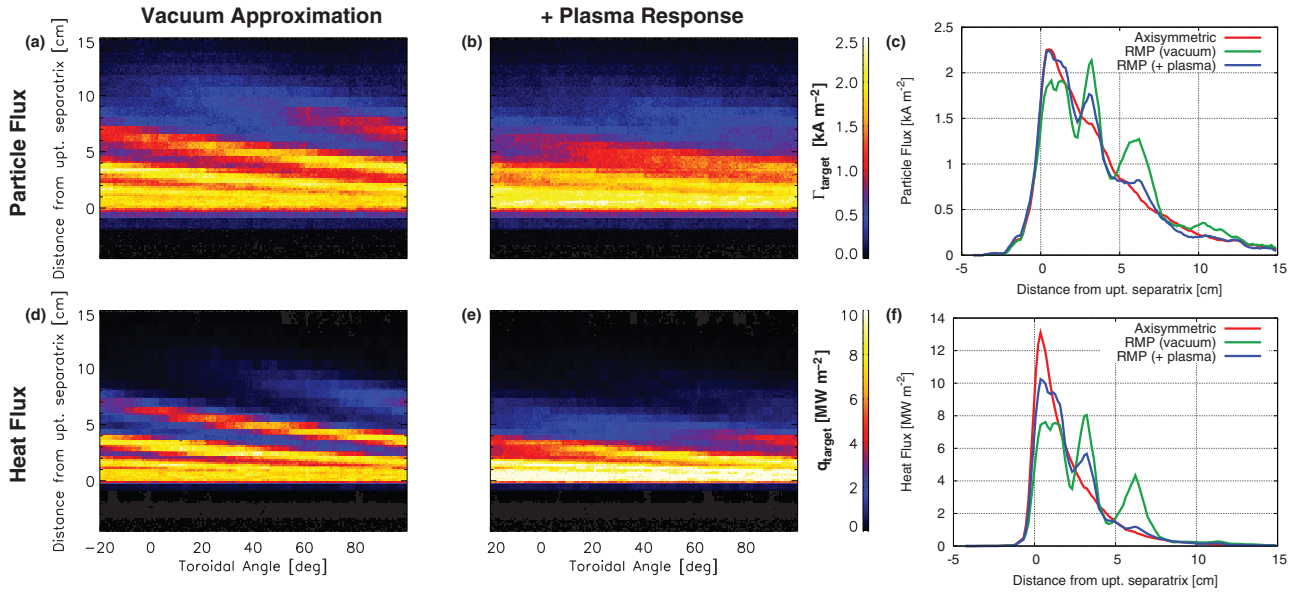

FIG. 7. (a)–(c) Target particle loads and (d)–(f) target heat loads at the inner strike point for the vacuum approximation and the plasma response case. Profiles are extracted in (c) and (f) at $\varphi = 0$ deg and compared to the axisymmetric configuration.

The third peaks (at $\Delta L \approx 6$ cm) are almost completely eliminated, down to the level of the axisymmetric configuration. A comparison with Figure 3 shows that these peaks are located at the strike location of a thin layer around the separatrix (blue region), i.e., the former scrape-off layer (SOL) of the axisymmetric configuration. The reason for this expanded particle and heat flux striation pattern observed in the simulation is cross-field transport into this layer, which is the regular mechanism in axisymmetric scrape-off layers. Such an expansion is also found in the "plasma response" case, where the second peak is already located in the regular SOL. Furthermore, there is also experimental evidence of this expansion by D_α and C_{II} light,[28] which is related to the target particle flux.

IV. CONCLUSIONS

A plasma response has been taken into account in 3D plasma edge transport simulations by an *ad hoc* screening of the external RMP field in the plasma up to the $q = 11/3$ surface at $\Psi_N = 0.96$. The implementation via helical current sheets on resonant magnetic surfaces is flexible enough to allow more realistic scenarios obtained from MHD modeling in the future. For the present assumption, it has been shown that the helical patterns in the plasma edge and on the divertor target are considerably modified compared to the vacuum approximation. The strong temperature reduction in the vacuum approximation can indeed be mitigated by RMP screening; however, the experimentally and numerically observed "density pump out effect" is then considerably weakened as well. Furthermore, a flat temperature profile persists in the remaining "open field line domain" inside the separatrix, which indicates that the parallel electron heat flux is overestimated in the fluid model. The beginning of this "open field line domain" is determined by the outermost screening surface; however, in case of partial screening, it may extend further inside. The secondary peak of the striated target heat flux is more reduced than the corresponding particle flux, which is in tendency the behavior expected from experimental observations.

ACKNOWLEDGMENTS

This work was supported in part by Grant No. GRT-055 (PMS-PE) of Fusion for Energy (ITA C19TD41FE) and by the U.S. Department of Energy under DE-FC02-04ER54698 and the Grant Agency of the Czech Republic under Grant No. P205/11/2341.

[1]T. E. Evans, R. K. W. Roeder, J. A. Carter, B. I. Rapoport, M. E. Fenstermacher, and C. J. Lasnier, J. Phys. Conf. Ser. **7**, 174 (2005).
[2]O. Schmitz, T. Evans, M. Fenstermacher, H. Frerichs, M. Jakubowski, M. Schaffer, A. Wingen, W. West, N. Brooks, K. Burrell, J. deGrassie, Y. Feng, K. Finken, P. Gohil, M. Groth, I. Joseph, C. Lasnier, M. Lehnen, A. Leonard, S. Mordijck, R. Moyer, A. Nicolai, T. Osborne, D. Reiter, U. Samm, K. Spatschek, H. Stoschus, B. Unterberg, E. Unterberg, J. Watkins, R. Wolf, and the DIII-D and TEXTOR Teams, Plasma Phys. Controlled Fusion **50**, 124029 (2008).
[3]M. Jakubowski, O. Schmitz, S. Abdullaev, S. Brezinsek, K. Finken, A. Krämer-Flecken, M. Lehnen, U. Samm, K. Spatschek, B. Unterberg, R. Wolf, and TEXTOR Team, Phys. Rev. Lett. **96**, 035004 (2006).
[4]O. Schmitz, M. Jakubowski, H. Frerichs, D. Harting, M. Lehnen, B. Unterberg, S. Abduallaev, S. Brezinsek, I. Classen, T. Evans, Y. Feng, K. Finken, M. Kantor, D. Reiter, U. Samm, B. Schweer, G. Sergienko, G. Spakman, M. Tokar, E. Uzgel, R. Wolf, and the TEXTOR Team, Nucl. Fusion **48**, 024009 (2008).
[5]J.-W. Ahn, R. Maingi, J. M. Canik, A. G. McLean, J. D. Lore, J.-K. Park, V. A. Soukhanovskii, T. K. Gray, and A. L. Roquemore, Phys. Plasmas **18**, 056108 (2011).
[6]E. Nardon, P. Cahyna, S. Devaux, A. Kirk, A. Alfier, E. D. L. Luna, G. D. Temmerman, P. Denner, T. Eich, T. Gerbaud, D. Harting, S. Jachmich, H. Koslowski, Y. Liang, Y. Sun, The MAST team and JET-EFDA Contributors, J. Nucl. Mater. **415**, S914 (2011).
[7]T. E. Evans, R. A. Moyer, P. R. Thomas, J. G. Watkins, T. H. Osborne, J. A. Boedo, E. J. Doyle, M. E. Fenstermacher, K. H. Finken, R. J. Groebner, M. Groth, J. H. Harris, R. J. L. Haye, C. J. Lasnier, S. Masuzaki, N. Ohyabu, D. G. Pretty, T. L. Rhodes, H. Reimerdes, D. L. Rudakov, M. J. Schaffer, G. Wang, and L. Zeng, Phys. Rev. Lett. **92**, 235003 (2004).
[8]T. E. Evans, R. A. Moyer, K. H. Burrell, M. E. Fenstermacher, I. Joseph, A. W. Leonard, T. H. Osborne, G. D. Porter, M. J. Schaffer, P. B. Snyder, P. R. Thomas, J. G. Watkins, and W. P. West, Nature Phys. **2**, 419 (2006).

[9]Y. Liang, H. R. Koslowski, P. R. Thomas, E. Nardon, B. Alper, P. Andrew, Y. Andrew, Arnoux, Y. Baranov, M. Becoulet, M. Beurskens, T. Biewer, M. Bigi, K. Crombe, E. D. L. Luna, P. de Vries, W. Fundamenski, S. Gerasimov, C. Giroud, M. P. Gryaznevich, N. Hawkes, S. Hotchin, D. Howell, S. Jachmich, V. Kiptily, L. Moreira, V. Parail, S. D. Pinches, E. Rachlew , and O. Zimmermann, Phys. Rev. Lett. **98**, 265004 (2007).
[10]W. Suttrop, T. Eich, J. C. Fuchs, S. Günter, A. Janzer, A. Herrmann, A. Kallenbach, P. T. Lang, T. Lunt, M. Maraschek, R. M. McDermott, A. Mlynek, T. Pütterich, M. Rott, T. Vierle, E. Wolfrum, Q. Yu, I. Zammuto, H. Zohm, and ASDEX Upgrade Team, Phys. Rev. Lett. **106**, 225004 (2011).
[11]A. Loarte, G. Saibene, R. Sartori, D. Campbell, M. Becoulet, L. Horton, T. Eich, A. Herrmann, G. Matthews, N. Asakura, A. Chankin, A. Leonard, G. Porter, G. Federici, G. Janeschitz, M. Shimada, and M. Sugihara, Plasma Phys. Controlled Fusion **45**, 1549 (2003).
[12]H. Frerichs, D. Reiter, O. Schmitz, T. E. Evans, and Y. Feng, Nucl. Fusion **50**, 034004 (2010).
[13]H. Frerichs, D. Reiter, O. Schmitz, D. Harting, T. E. Evans, and Y. Feng, "On gas flow effects in 3D edge transport simulations for DIII-D plasmas with resonant magnetic perturbations," Nucl. Fusion **52**, 054008 (2012).
[14]J. Lore, J. Canik, Y. Feng, J.-W. Ahn, R. Maingi, and V. Soukhanovskii, "Implementation of the 3D Edge Plasma Code EMC3-EIRENE on NSTX," Nucl. Fusion **52**, 054012 (2012).
[15]T. Lunt, Y. Feng, M. Bernet, A. Herrmann, P. Marne, R. McDermott, H. Müller, S. Potzel, T. Pütterich, S. Rathgeber, W. Suttrop, E. Viezzer, E. Wolfrum, M. Willensdorfer, and the ASDEX Upgrade Team, "First EMC3-EIRENE simulations of the edge magnetic perturbations at ASDEX Upgrade compared with the experiment," Nucl. Fusion **52**, 054013 (2012).
[16]P. Cahyna, E. Nardon, JET EFDA Contributors, J. Nucl. Mater. **415**, S927 (2011).
[17]M. F. Heyn, I. B. Ivanov, S. V. Kasilov, W. Kernbichler, I. Joseph, R. A. Moyer, and A. M. Runov, Nucl. Fusion **48**, 024005 (2008).
[18]H. Stoschus, O. Schmitz, H. Frerichs, M. W. Jakubowski, B. Unterberg, S. S. Abdullaev, M. Clever, J. W. Coenen, U. Kruezi, D. Schega, U. Samm, and TEXTOR Research Team, Phys. Plasmas **17**, 060702 (2010).
[19]E. Nardon, P. Tamain, M. Becoulet, G. Huysmans, and F. L. Waelbroeck, Nucl. Fusion **50**, 034002 (2010).
[20]Y. Feng, F. Sardei, J. Kisslinger, and P. Grigull, J. Nucl. Mater. **241–243**, 930 (1997).
[21]Y. Feng, F. Sardei, J. Kisslinger, P. Grigull, K. McCormick, and D. Reiter, Contrib. Plasma Phys. **44**(1–3), 57 (2004).
[22]M. Kobayashi, Y. Feng, F. Sardei, D. Reiter, K. Finken, and D. Reiser, Nucl. Fusion **44**, S64 (2004).
[23]O. Schmitz, D. Harting, S. Abdullaev, S. Brezinsek, K. Finken, H. Frerichs, M. Jakubowski, M. Lehnen, X. Loozen, P. Mertens, D. Reiter, U. Samm, B. Schweer, G. Sergienko, M. Tokar, B. Unterberg, R. Wolf, and the TEXTOR Team, J. Nucl. Mater. **363–365**, 680 (2007).
[24]H. Frerichs, M. Clever, Y. Feng, M. Lehnen, D. Reiter, and O. Schmitz, Nucl. Fusion **52**, 023001 (2012).
[25]H. Frerichs, D. Reiter, Y. Feng, and D. Harting, Comp. Phys. Commun. **181**, 61 (2010).
[26]M. Z. Tokar, T. E. Evans, R. Singh, and B. Unterberg, Phys. Plasmas **15**, 072515 (2008).
[27]T. E. Evans, R. A. Moyer, and P. Monat, Phys. Plasmas **9**, 4957 (2002).
[28]O. Schmitz, T. Evans, M. Fenstermacher, A. McLean, J. Boedo, N. Brooks, H. Frerichs, M. Jakubowski, R. Laengner, C. Lasnier, A. Loarte, R. Moyer, D. Orlov, H. Reimerdes, D. Reiter, U. Samm, H. Stoschus, E. Unterberg, J. Watkins, and the DIII-D and TEXTOR Teams, J. Nucl. Mater. **425**, S886 (2011).
[29]S. I. Braginskii, "Transport processes in a plasma," in *Reviews of Plasma Physics*, edited by M. A. Leontovich (Consultants Bureau, New York, 1965), Vol. 1, 205–311.
[30]O. Schmitz, T. E. Evans, M. E. Fenstermacher, E. A. Unterberg, M. E. Austin, B. D. Bray, N. H. Brooks, H. Frerichs, M. Groth, M. W. Jakubowski, C. J. Lasnier, M. Lehnen, A. W. Leonard, S. Mordijck, R. A. Moyer, T. H. Osborne, D. Reiter, U. Samm, M. J. Schaffer, B. Unterberg, W. P. West, and the DIII-D and TEXTOR Research Teams, Phys. Rev. Lett. **103**, 165005 (2009).
[31]V. Rozhansky, E. Kaveeva, P. Molchanov, I. Veselova, S. Voskoboynikov, D. Coster, A. Kirk, S. Lisgo, and E. Nardon, Nucl. Fusion **50**, 034005 (2010).
[32]J. Coenen, O. Schmitz, B. Unterberg, M. Clever, M. Jakubowski, U. Samm, B. Schweer, H. Stoschus, M. Tokar, and the TEXTOR-Team, Nucl. Fusion **51**, 063030 (2011).